Article

Removal of Uranium and Associated Contaminants from Aqueous Solutions Using Functional Carbon Nanotubes-Sodium Alginate Conjugates

Hussein Allaboun [1,2,*], Mohammad M. Fares [3] and Fahmi A. Abu Al-Rub [1]

[1]   Department of Chemical Engineering, Faculty of Engineering, Jordan University of Science and Technology, P.O. Box 3030, Irbid 22110, Jordan; abualrub@just.edu.jo
[2]   Jordan Atomic Energy Commission, P.O. Box 70, Amman 11934, Jordan
[3]   Department of Chemical Sciences, Faculty of Science & Arts, Jordan University of Science and Technology, P.O. Box 3030, Irbid 22110, Jordan; fares@just.edu.jo
*   Correspondence: allaboun@just.edu.jo; Tel.: +962-79-588-5280

Abstract: Synthesis of hydrophilic/hydrophobic beads from functional carbon nanotubes (CNTs) conjugated with sodium alginate was investigated. Glutaraldehyde was used as a coupling agent and Ca^{2+} as a crosslinking agent. The formed conjugate comprises two-dimensional sheets of sodium alginate bounded to long tufts of functional CNT tails of micro-size geometry. Detailed characterization of the conjugates was performed using thermogravimetric analysis (TGA) and its first derivative (DTG), Fourier transform infrared (FTIR), and scanning electron microscope (SEM) techniques. Different ratios of the conjugate were successfully prepared and used as biodegradable environmentally friendly sorbents. Removal of U^{6+}, V^{3+}, Cr^{3+}, Mo^{3+}, Pb^{2+}, Mn^{2+}, Cu^{2+}, Ti^{4+} and Ni^{2+} from aqueous solutions using the synthesized biosorbent was experimentally demonstrated. Maximum metal uptake of 53 mg/g was achieved using the % Functional CNTs = 33 sample.

Keywords: functional CNT-sodium alginate beads; uranium tailings; water purification; industrial effluents; environmentally friendly biosorbents; hydrophilic/hydrophobic

1. Introduction

Profound cost benefit analyses for many novel materials appearing in the world endorse carbon nanotubes (CNTs) as the Trojan horse in the nanotechnology race. Due to their extraordinary properties, many industries could effectively use CNTs and its derivatives in a wide range of versatile applications: National Aeronautics and Space Administration (NASA) utilizes CNTs as sensors for gas detection [1], IBM in high performance electronics [2,3], and INTEL in delicately engineered nanowires [4]. In addition, CNTs have already been incorporated in the manufacturing of energy storage technologies [5], electron field emitting displays [6], fuel cells [7,8], and semiconductors [9,10]. In the field of bio-applications, CNTs receive considerable attention in radio-diagnosis imaging [11,12], cancer therapy and other therapies as drug carriers [13–18], and in detection and binding of DNA and RNA [19–22]. CNTs are also acknowledged for their high adsorption affinity towards: (1) organic pollutants such as aniline and phenol via non-covalent forces, such as π–π stacking, van der Waals forces, and hydrophobic interactions [23] and (2) multivalent environmental ion contaminants over a broad range of pH values [24,25]. Currently, CNTs account for 28% of the overall global market demand of nanomaterials with a proposed production of up to 12,766 metric tons by 2016 [26].

On the other hand, naturally occurring polymers modified via synthetic routes are gaining widespread applications especially in biomaterials as smart and stimuli-sensitive drug delivery

systems [27–35], in biosorption processes [36,37], and in protective coatings of metal surfaces [38–41]. Moreover, these materials such as sodium alginate are gaining promising futuristic anticipations not only due to their capability to adhere to biological tissues but also due to their biodegradable and environmentally friendly characteristics [42]. Iron oxide loaded alginate beads have been investigated for the removal of arsenic from contaminated water. Three types of modified alginate beads were studied, and a preferential behavior to adsorb As(V) was reported. As(III) was found to be less efficiently adsorbed [43].

Nevertheless, water purification is materializing as one of the major widespread dilemmas of the industrial world. The purification of drinking water and wastewater arouse as paramount issues throughout the uprising environmental threats and the global water-shortage crisis. To purify water from uranium and other contaminants, a multitude of techniques are being administered [44]. This research investigates the opportunity to purify water by harnessing the power attained when the characteristics of both synthetically modified CNTs and alginate are combined together. The proposed conjugate is deemed conceivable by modulating the sidewall surfaces of CNTs via the insertion of a carboxylic acid functional group into their backbone structure. The described implantation renders the CNTs ready to couple with the synthetically modified alginate and enhances the molecules surface area characteristics and suspension performance in aqueous solutions.

This research is dedicated to develop environmentally friendly beads of surface enhanced CNTs bounded to naturally occurring alginate. Such biosorbents are favorable due to their biodegradability, hydrophobic/hydrophilic surface characteristics, and high efficiency biosorption characteristics. The formed novel biosorbents which come with micro-size geometry were characterized via thermogravimetric analysis (TGA), Fourier transform infrared (FTIR) and scanning electron microscope (SEM) techniques, and were further evaluated experimentally for their capability to purify water from dissolved uranium and other multivalent heavy metal pollutants.

2. Experimental

2.1. Materials

Multi-walled CNTs purchased from NanocylTM NC7000, Sambreville, Belgium. Sodium alginate, a gluteraldehyde cross-linker, was purchased from Acros organics, Geel, Belgium. Multicomponent ICP (Inductively Coupled Plasma) standard was purchased from AccuStandard, New Haven, CT, USA. The other reagents were analytical grade and used as received.

2.2. Investigation Tools

Thermogravimetric Analysis (TGA) (Netzsch Proteus, Selb, Germany) thermograms performed under N_2 atmosphere at a heating rate of 10 °C/min in 25–900 °C temperature range. FTIR: Shimadzu IRAffinity-1 FTIR spectrophotometer (Shimadzu, Tokyo, Japan) recorded the vibrational spectra in the 4000–400 cm^{-1} range using KBr pellets. Scanning Electron Microscopy (SEM); the samples were coated with gold ion by sputtering method with (DSM 950 (ZEISS) model) (ZEISS, Pleasanton, CA, USA), (E6100) model (Polaron (now Quorum Technologies, Laughton, UK)). Inductively Coupled Plasma Mass Spectrometry (ICP-MS) (Elan DRC-E (Dynamic Reaction Cell-Enhanced) by PerkinElmer Sciex (Concord, ON, Canada), used to analyze aqueous samples resulted from purification of contaminated water evaluation.

2.3. Acid Functionalized Carbon Nanotubes (CNTs)

In a 50 mL dried round bottom flask equipped with a condenser, 0.5 g multi-walled carbon nanotubes (CNTs) dispersed in 40 mL of 9.0 M nitric acid and refluxed for 8.0 h for three rounds at 75–80 °C. The use of 9.0 M nitric acid meant to increase the defect sites and –COOH groups and at the same time maintain appropriate yield for the oxidation process [45]. The solution was allowed to cool down to ambient temperature and then a large volume of deionized water was added to

the resultant dispersed solution. The functionalized CNTs were collected by filtration whereas the remained suspended portion was separated by centrifugation. In order to remove any amounts of trapped nitric acid, the produced functionalized CNT sample was thoroughly washed with deionized water until a neutral pH value of the filtrate was observed. The product was dried overnight at 40 °C.

2.4. Functional CNT-Alginate Beads

As part of this experiment, 200 mg sample of functional CNTs dispersed in 20 mL deionized water, and in another flask, 200 mg sodium alginate (SA) dispersed in 20 mL aqueous solution. The sodium alginate solution was slowly poured into the functional CNT dispersed solution under continuous stirring. Then, 40 mg acidified glutaraldehyde solution, acting as coupling agent, was added to the mixture. The mixture stirred at 40 °C for 60 min until one homogenous dense black phase was formed. The dense solution was added dropwise, through a dropper, into large volume of 2% (w/w) $CaCl_2$ solution, where Ca^{2+} acted as a crosslinking agent. Immediate formation of bead-like agglomerations of the functional CNT-sodium alginate conjugate was observed. The formed beads are left in solution for 24 h to achieve complete nucleation, and then filtered and flushed thoroughly with distilled water to remove any uncross linked and unreacted dispersions of functional CNTs or alginate moieties. The average size of the beads is approximately 5 mm in diameter. To serve the purpose of this research, the following four different functional CNT samples were prepared and subjected to bench-scale laboratory testing:

Table 1. List of synthesized % functional carbon nanotubes (CNT) samples.

Sample	Functional CNTs (%)
I	17
II	33
III	50
IV	100

The fraction of functional CNTs (in %) in the functional CNT-sodium alginate beads were calculated from the following relation:

$$\text{Functional CNT (\%)} = \frac{\text{AUC}_{\text{CNTs}}}{\left(\text{AUC}_{\text{CNTs}} + \text{AUC}_{\text{alginate}}\right)} \times 100 \tag{1}$$

where AUC_{CNTs} and $\text{AUC}_{\text{alginate}}$ represent the area under the curves of functional CNTs and sodium alginate (SA) moieties, respectively. The area under the curves was determined from the first derivative thermogravimetric analysis technique (TGA) using the software package provided by Derivative Thermogravimetric (DTG) thermogram in a similar manner to previously reported work [34,36].

2.5. Removal of Uranium and Other Contaminants

Two liters of multicomponent (Ni^{2+}, Ti^{4+}, Cu^{2+}, Mn^{2+}, Pb^{2+}, Mo^{3+}, Cr^{3+}, V^{3+} and U^{6+}) solution of 50 ppm concentration was prepared by diluting 100 mL of AccuStandard multicomponent solution with ASTM I (Ultra-pure) water. The concentration of each species in original standard is 1000 ppm. In a 500 mL bottle, 2 mL of wet functional CNT-sodium alginate beads (obtained from 2.4) was mixed with 300 mL multicomponent solution (species concentration 50 ppm). Four bottles were prepared—one for each type of the synthesized beads (Table 1). The bottles were placed on a rotating bottle device and rolled for 5 h; afterwards, the mixture was filtered. While still on the filter paper, the beads were washed with 20 mL of ASTM I (Ultra-pure) water to ensure no entrainment existed. The resulting combined solution of filtrate mixed with the wash was sent for assaying by ICP-MS. The experiment was repeated but for a contact time of 24 h; no enhancement in adsorption was observed.

3. Results and Discussion

3.1. Structural Identification of Functional CNT-Alginate Conjugates

The conjugate formulation of a biosorbant is based on a two-step consecutive crosslinking process of the negatively charged carboxylate group (COO–) located on the surface of alginate macromolecule and the surface enhanced functional CNT thread. The addition of gluteraldehyde acidified with two drops of 1.0 M hydrochloric acid guarantees the immediate formation of double-sided positive charges on the gluteraldehyde molecule. Such ion species act as a coupling agent of the negative charge carboxylate groups (COO–) located on the surfaces of alginate macromolecule and functional CNT thread, leading to the formation of micro-size geometry as depicted in Scheme 1. Consecutively, the addition of calcium ion species (Ca^{2+}) in aqueous solution, acting as a crosslinking agent, tends to bind micro-size geometry freely distributed in solution with each other to form spherical beads. The shell of beads probably will form hydrophilic surfaces of alginate macromolecules, whereas the core of beads will be formed of hydrophobic functional CNT threads.
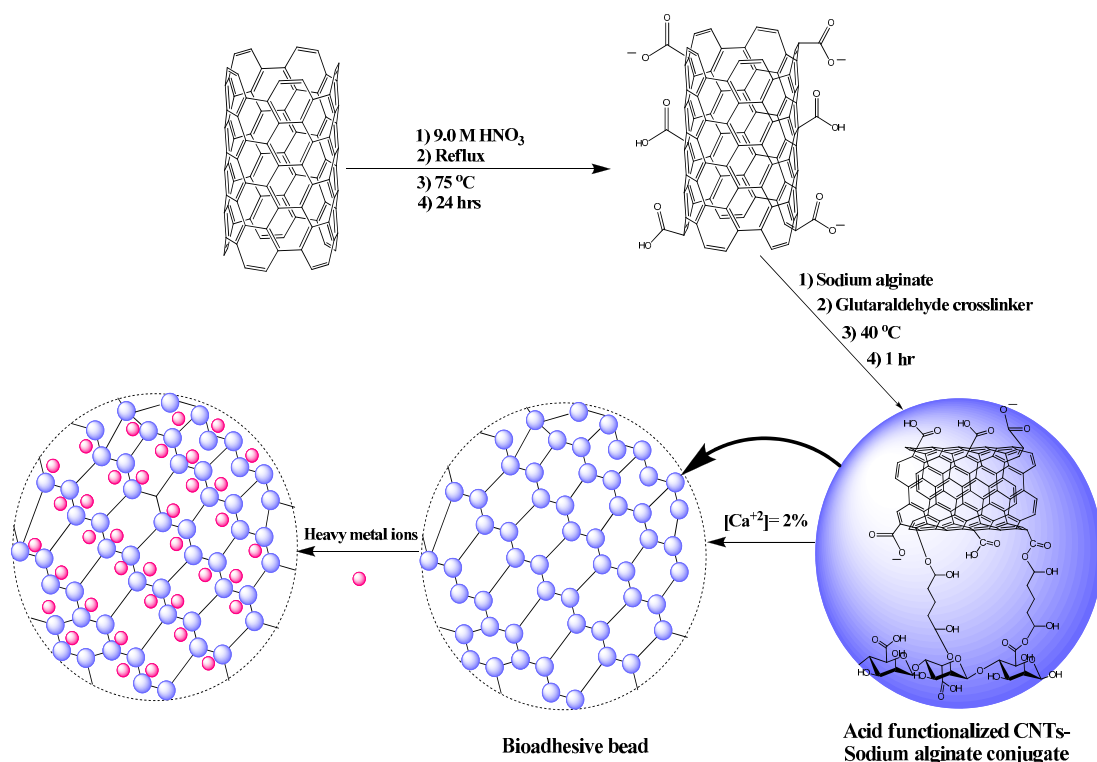

Scheme 1. Schematic illustration of the synthesis process for conjugates and beads.

The foremost distinctive features of thermogravimetric analysis thermograms, TGA, and its first derivative, DTG, techniques are thermal stability and decomposition temperature of the formed conjugates. Figure 1a shows the first derivative thermogram of the as received carbon nanotubes before being acid functionalized. No degradation peaks were observed up to 900 °C. This confirms high thermal stability and high resistance against thermal degradation up to 900 °C. On the other hand, Figure 1b shows distinctive and broad decomposition peak for functional CNTs at 693 °C. The lower decomposition temperature of functional CNTs with respect to as-received CNTs confirm the appearance of defects and oxidizable fractions, which result from the oxidation process during acid treatment, on the surface of carbon nanotubes that weaken the entire structure of CNTs. In other words, the oxidation processes of CNTs include the formation of carboxylic acid groups (COOH) on the sides of the CNT cylinders. Such groups deprotonate and form carboxylate ions (COO–) at pH = 7.0, which repel each other and lead to weaker intermolecular forces (*i.e.*, weaker π–π stacking,

van der Waals forces and hydrophobic interactions). This weakness causes the observed lower decomposition temperature.

However, sodium alginate shows sharp midpoint decomposition peak at 242 °C as seen in Figure 1c. At the splitting of the first derivative peak, the DTG is attributed to two types of alginate: bulk, non-conjugated alginate and conjugated alginate. Interestingly, the decomposition peak of sodium alginate in the functional CNT-sodium alginate conjugate (Figure 1d) appears at the same decomposition temperature as in Figure 1c, whereas, the decomposition temperature of functional CNTs increased to 807 °C. This extremely large increase in decomposition temperature (*i.e.*, 114 °C) is attributed to the large surface area of functional CNT threads that allow easy and large crosslinking, via glutaraldehyde and calcium ion, which eventually leads to stronger and more consistent CNT threads and hence more thermally stable constructions. Any carboxylate group not functionalized will also exist as calcium salts at this point as well, thereby increasing the decomposition temperature. However, the insignificant increase in decomposition temperature of alginate fraction is due to geometric planar properties of alginate [46] that tend to form dominant self-aggregate layers which were not strongly incorporated in the crosslinking process.
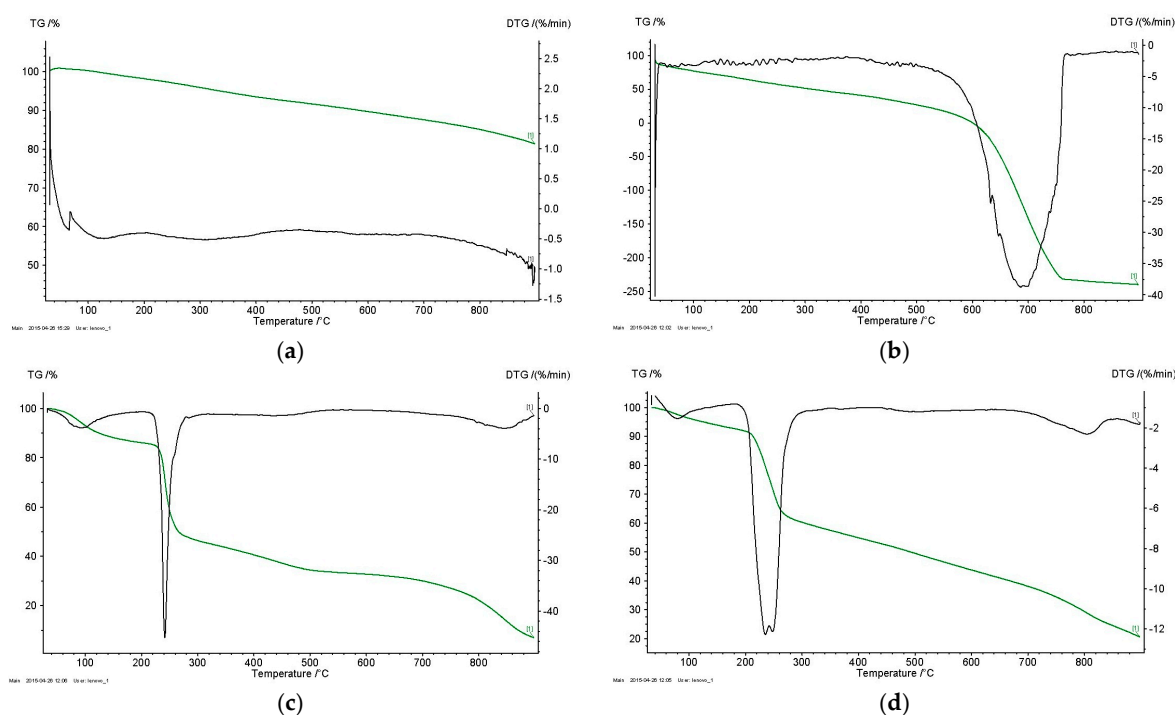
Figure 1. Thermogravimetric analysis (TGA) thermogram and its first derivative (DTG) of: (**a**) as-received CNTs, (**b**) functional CNTs, (**c**) sodium alginate, and (**d**) functional CNT-sodium alginate conjugate (% Functional CNTs = 17).

Figure 2 and Table 2 illustrate the FTIR stretchings for the functional CNTs and the functional CNT-sodium alginate conjugates. In the functional CNT spectrum, apparently, the presence of characteristic peaks of carbonyl, asymmetric and symmetric carboxyl and hydroxyl stretchings located respectively at 1735, 1638, 1387 and 3443 cm^{-1}, provide evidence of successful acid functionlization of CNT threads. In addition, asymmetric CH stretching of methyl bounded to aromatic groups, and symmetric CH stretching of methyl and methylene groups located respectively at 2960, 2922 and 2851 cm^{-1}, provide other evidence of successful acid functionlization of CNTs by nitric acid. Furthermore, the larger intensified hydroxyl (OH) band at 3443 cm^{-1} in the functional CNTs-sodium alginate conjugate refers to the presence of hydroxyl groups from alginate and crosslinker, respectively. Moreover, the carbonyl, asymmetric carboxyl, and symmetric carboxyl stretchings are intensified in

the functional CNT-sodium alginate conjugate as described in Table 2. The presence of carboxyl groups bearing negative charge in the functional CNT-sodium alginate conjugates are important to hook and trap positive charge multivalent environmental ion contaminants, and hence play a dominant key role in the biosorption process.
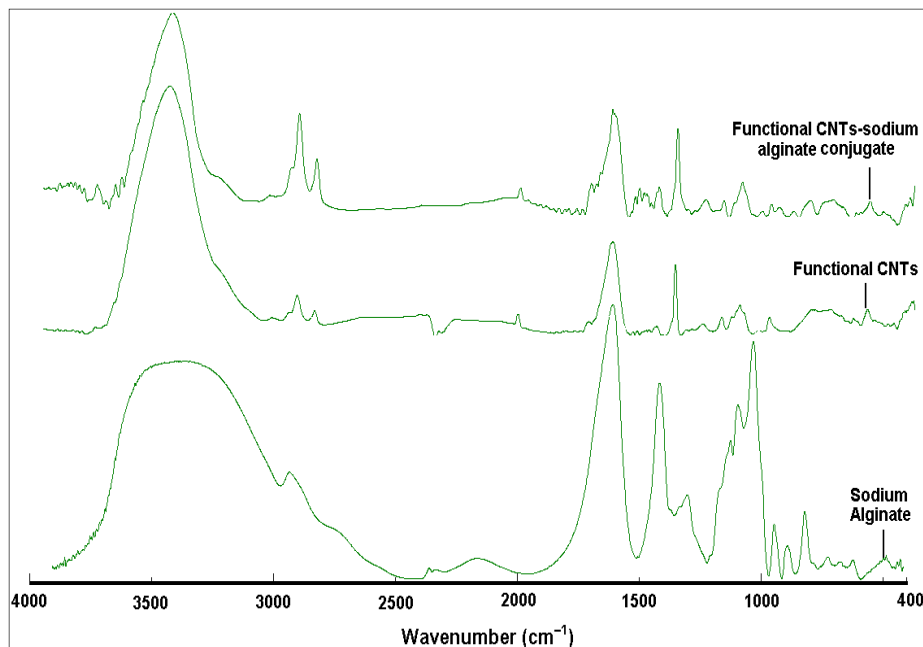
Figure 2. Fourier transform infrared (FTIR) spectra of sodium alginate, functional CNTs and functional CNT-sodium alginate conjugate.

Table 2. Characteristic Fourier transform infrared (FTIR) peaks of functional CNTs and functional CNT-sodium alginate conjugate.

Composite	Wavenumber (cm^{-1})	Absorbance	Functional Group	Reference
Functional CNTs	3443	0.003	OH stretching	[47,48]
	2960	0.074	Asymmetric CH stretching of methyl groups	[47,48]
	2922	0.073	Asymmetric CH stretching of methyl bounded to aromatic groups	[49,50]
	2851	0.077	Symmetric CH stretching of methyl and methylene groups	[47–50]
	1735	0.087	C=O stretching	-
	1638	0.069	Asymmetric COO– stretching	-
	1557	0.089	C=C stretching	[51]
	1387	0.072	Symmetric COO– stretching	[52]
Functional CNTs-alginate conjugates	3443	0.096	OH stretching	-
	2960	0.160	Asymmetric CH stretching of methyl groups	-
	2922	0.149	Asymmetric CH stretching of methyl bounded to aromatic groups	-
	2851	0.159	Symmetric CH stretching of methyl and methylene groups	-
	1735	0.164	C=O stretching	-
	1638	0.144	Asymmetric COO stretching	-
	1557	0.157	C=C stretching	-
	1387	0.152	Symmetric COO stretching	-

Scanning electron microscope (SEM) images was utilized to identify and describe the surface topology of the functional CNT samples pre- and post-conjugation with sodium alginate (Figure 3). The as-received carbon nanotubes (CNTs) in Figure 3a show cylindrical shape yarns and threads accumulated above each other forming longitudinal clusters. The free volume between the threads

is obviously small. As the oxidation occurs, the CNTs are more dispersible in water as the aromatic trunks become more hydrophilic. This allows a better dispersion and minimizes the agglomeration that occurs in aqueous solutions. Free volume between threads became larger, and the cluster structure got loosened and disassembled as shown in Figure 3b. This could also be due to the presence of negatively charged carboxylate groups that allow repulsion between CNT cylinders and hence the formation of a larger free volume structure. The widely spread functional carbon nanotubes threads and the largely created free volume increase the microscopic surface area available for biosorption of positive charge metals and ion chelating.


(**a**)   (**b**)
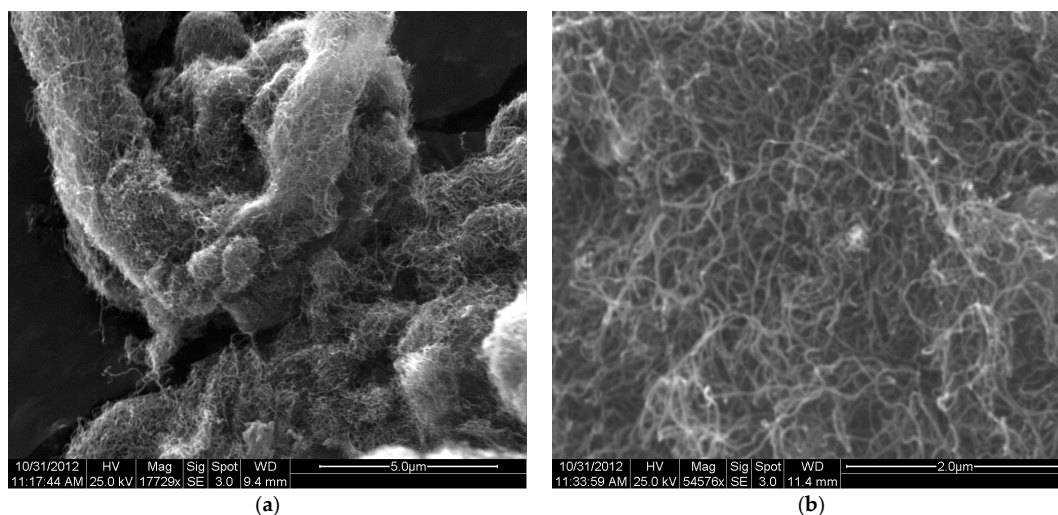
Figure 3. Surface topology by SEM images of the functional CNT samples pre- and post-conjugation with sodium alginate: (**a**) as-received CNTs; (**b**) functional CNTs = 100%.

Sodium alginate demonstrated two-dimensional sheet microstructures as shown in Figure 4a. In the Figure 4b–d, functional CNT-sodium alginate conjugates demonstrated two-dimensional sheets of sodium alginate cross-linked with scattered CNT threads. Such scattering of functional CNTs bounded to the alginate sheets is critical for the success of the biosorption processes. It allows less-constrained diffusion pathways for dissolved ions to follow in pursuit of available landing sites.

(**a**)   (**b**)
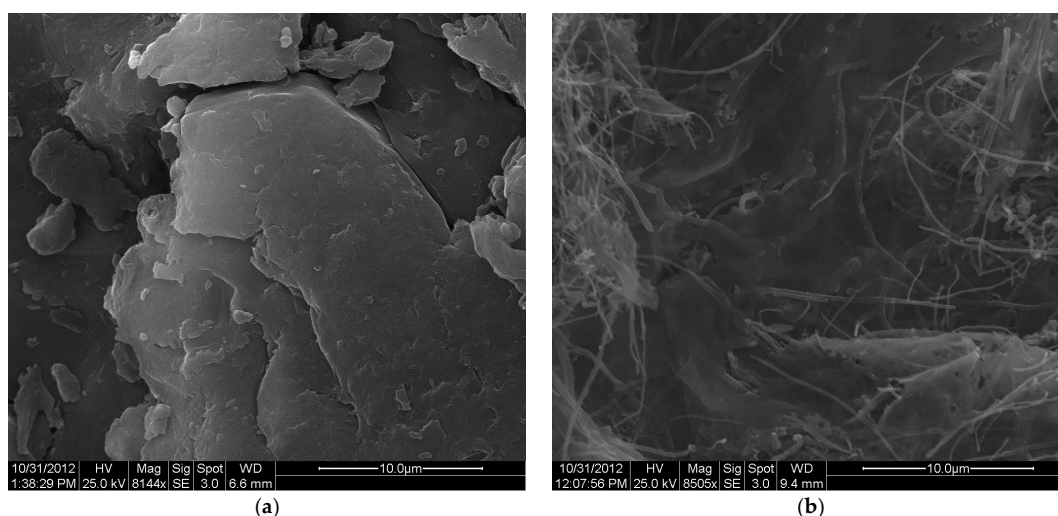
Figure 4. *Cont.*
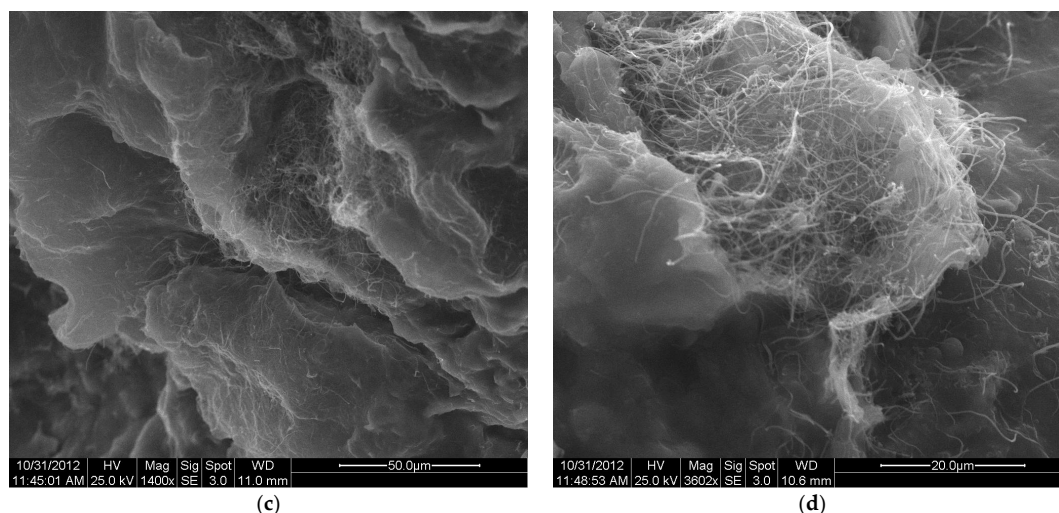
Figure 4. SEM images showing Sodium Algenate microstructure for the various synthesized % Functional CNTs: (**a**) Sodium alginate sheets; (**b**) Functional CNT-sodium alginate conjugates (% of Functional CNTs = 50); (**c**) and (**d**) Functional CNT-sodium alginate conjugates (% of Functional CNTs = 17).

3.2. Removal of Uranium and Associated Contaminants Using the Synthesized Biosorbent

The ability of the generated four types of functional CNT-sodium alginate beads to purify contaminated water was experimentally evaluated using synthesized aqueous solution containing the following nine co-existing multivalent ion pollutants: Ni^{2+}, Ti^{4+}, Cu^{2+}, Mn^{2+}, Pb^{2+}, Mo^{3+}, Cr^{3+}, V^{3+} and U^{6+}. The concentration of each species of these inorganic heavy metal ion pollutants in the solution was set to 50 ppm. The process of biosorption was allowed 5 h of continuous contact time between the beads and the aqueous solution. The biosorbents achieved variant intervention based on their different functional CNT content and hence acted differently depending on micro-size geometry and free volume between CNT threads in the aqueous solution. The recovery of these common environmental ion contaminants by the beads was measured by inductively coupled plasma mass spectrometry (ICP-MS) technology at pH = 6 and ambient temperature using the following relation:

$$q_e = \frac{(C_0 - C_e)\,V}{w} \tag{2}$$

where q_e is the equilibrium uptake (mg/g), C_0 is the initial ion contaminant concentration (mg/L), C_e is the equilibrium ion contaminant concentration (mg/L), V is the volume of the solution (L) and w is the mass of the conjugate (g).

Simultaneous considerable separation for the co-existing and competing ions from the aqueous solution was measured and the corresponding recoveries were calculated (Table 3 and Figure 5). However, no biosorbtion selectivity was demonstrated by any specific species amongst the array of used ions in spite of their different charge and size. This behavior alludes to the fact that the mechanism of the recovery process comprises sweeping physical adsorption of the positive charge ions in solution on the negative charge surface of the hydrophilic/hydrophobic beads. This behavior clearly indicates that carboxylate ions (COO–) located on the surface of functional CNT/Alginate conjugates play a dominant role in the biosorption process.

In total, the designed conjugate achieved a collective recovery of 53 mg/g metal ion uptake for the various ion contaminants that co-existed in the solution. Apparently, as the % of functional CNTs increases the metal ion uptake increases and then exponentially decreases. For the % functional CNTs = 17 sample, lower ion pollutant recovery was observed. This is due to the two-dimensional sheet geometry of the alginate that prevents the penetration and the adsorption of ions on the surface

of these sheets. On the other hand, smaller free volume between threads for the % of functional CNTs = 100 sample with respect to % of functional CNTs = 17 sample. This inhibited the penetration of environmental ion contaminants from reaching active adsorption sites, and hence, an obvious decrease in the efficiency towards metal ion biosorption is experienced. Hence, an obvious decrease in the efficiency towards metal ion biosorption is experienced. Maximum ion biosorption recovery was achieved using % of functional CNTs = 33 sample. This is believed to occur due to larger free volume between threads of indicated sample; the micro-size structures guarantee largest surface area of carboxylate groups oriented toward the solution and, therefore, achieved the maximum metal ion biosorption. Moreover, the hydrophobic/hydrophilic characteristics of the conjugate micro-size geometry, revealed from hydrophobic CNT threads and hydrophilic alginate sheets, adapted them to adsorb inorganic heavy metal ion pollutants. This may present these conjugates to strongly act as universal inorganic and organic biosorbents.
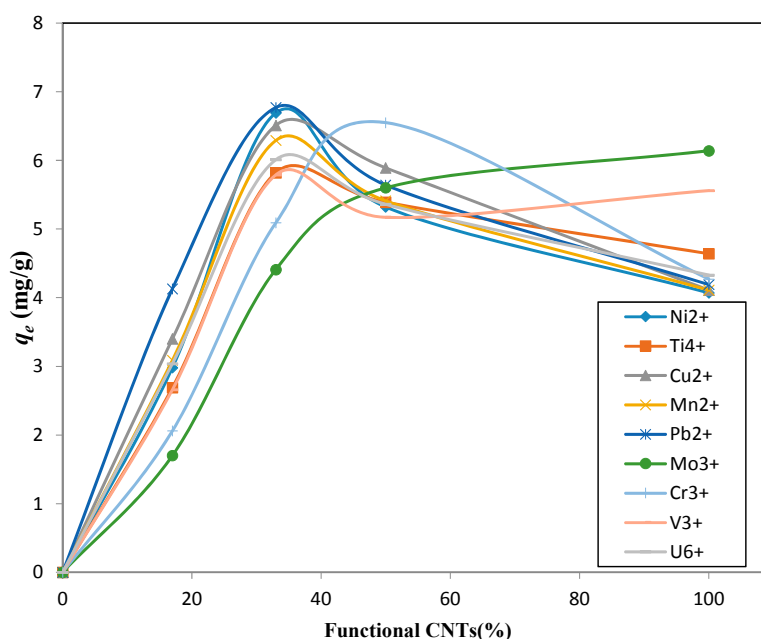
Figure 5. Change in recovery of environmental ion contaminants against different functional CNT bead samples.

Table 3. Environmental ion contaminants recovery (q_e) (mg/g) using different functional CNT content conjugates.

Functional CNTs (%)	Ni^{2+}	Ti^{4+}	Cu^{2+}	Mn^{2+}	Pb^{2+}	Mo^{3+}	Cr^{3+}	V^{3+}	U^{6+}
17	2.98	2.69	3.40	3.09	4.13	1.70	2.06	2.66	3.04
33	6.69	5.82	6.51	6.29	6.77	4.41	5.09	5.79	6.01
50	5.32	5.39	5.89	5.41	5.64	5.60	6.55	5.17	5.36
100	4.07	4.64	4.11	4.11	4.19	6.14	4.27	5.56	4.33

4. Conclusions

Beads of acid-functionalization carbon nanotubes conjugated with sodium alginate were synthesized. The use of glutaraldehyde and Ca^{2+} profoundly enhanced respective coupling and crosslinking properties of the formed micro-structure. Detailed characterization using TGA, DTGA, FTIR and SEM techniques, revealed the formation of hydrophilic/hydrophobic beads with two-dimensional sheets of alginate and long tufts of functional CNT tails. The synthesized four types of beads acted as novel biosorbents to dissolved uranium and other common industrial water pollutants. Low metal biosorption occurred at low and high % functional CNT bead types. Maximum

metal ion uptake was obtained for functional CNT = 33% sample. Metal recovery was found to be sensitive to available free volume between functional CNT threads. The hydrophilic/hydrophobic surface properties of the biodegradable conjugates together with the micro-size geometry adapt them to act as effective biosorbents for the purification of industrial water tailings.

Author Contributions: The three authors conceived and designed the experiments. Hussein Allaboun conducted the uranium removal experiments. Mohammad M. Fares performed the synthesis and characterization experiments. Fahmi A. Abu Al-Rub analyzed the data and discussed the results. Hussein Allaboun and Mohammad M. Fares wrote the paper.

Conflicts of Interest: The authors declare no conflict of interest.

References

1. Ames Technology Capabilities and Facilities. Available online: http://www.nasa.gov/centers/ames/research/technology-onepagers/gas_detection.html (accessed on 28 January 2016).

2. Cao, Q.; Han, S.-J.; Tulevski, G.S.; Zhu, Y.; Lu, D.D.; Haensch, W. Arrays of single-walled carbon nanotubes with full surface coverage for high-performance electronics. *Nat. Nanotechnol.* **2013**, *8*, 180–186. [CrossRef] [PubMed]

3. Franklin, A.D.; Tulevski, G.S.; Han, S.-J.; Shahrjerdi, D.; Cao, Q.; Chen, H.-Y.; Wong, H.-S.P.; Haensch, W. Variability in carbon nanotube transistors: Improving device-to-device consistency. *ACS NANO* **2012**, *6*, 1109–1115. [CrossRef] [PubMed]

4. Prasher, R.; Tong, T.; Majumdar, A. Approximate analytical models for phonon specific heat and ballistic thermal conductance of nanowires. *Nano Lett.* **2008**, *8*, 99–103. [CrossRef] [PubMed]

5. Frackowiak, E.; Gautier, S.; Gaucher, H.; Bonnamy, S.; Beguin, F. Electrochemical storage of lithium in multiwalled carbon nanotubes. *Carbon* **1999**, *37*, 61–69. [CrossRef]

6. Kurt, R.; Bonard, J.-M.; Karimi, A. Morphology and field emission properties of nano-structured nitrogenated carbon films produced by plasma enhanced hot filament CVD. *Carbon* **2001**, *39*, 1723–1730. [CrossRef]

7. Kannan, A.M.; Kanagala, P.; Veedu, V. Development of carbon nanotubes based gas diffusion layers by *in situ* chemical vapor deposition process for proton exchange membrane fuel cells. *J. Power Sour.* **2009**, *192*, 297–303. [CrossRef]

8. Sharma, T.; Reddy, A.L.M.; Chandra, T.S.; Ramaprabhu, S. Development of carbon nanotubes and nanofluids based microbial fuel cell. *Inter. J. Hydrog. Energy* **2008**, *33*, 6749–6754. [CrossRef]

9. Chang, J.; Lee, J.-H.; Najeeb, C.K.; Nam, G.-H.; Lee, M.; Kim, J.-H. Area-selective growth of ZnO nanorod arrays on single-walled carbon nanotube patterns. *Scr. Mater.* **2010**, *63*, 520–523. [CrossRef]

10. Lyu, S.C.; Zhang, Y.; Ruh, H.; Lee, H.J.; Lee, C.J. Synthesis of high-purity GaP nanowires using a vapor deposition method. *Chem. Phys. Lett.* **2003**, *67*, 717–722. [CrossRef]

11. Hong, S.Y.; Tobias, G.; Al-Jamal, K.T.; Ballesteros, B.; Ali-Boucetta, H.; Lozano-Perez, S.; Nellist, P.D.; Sim, R.B.; Finucane, C.; Mather, S.J.; *et al.* Filled and glycosylated carbon nanotubes for *in vivo* radioemitter localization and imaging. *Nat. Mater.* **2010**, *9*, 485–490. [CrossRef] [PubMed]

12. Welsher, K.; Sherlock, S.P.; Dai, H. Deep-tissue anatomical imaging of mice using carbon nanotube fluorophores in the second near-infrared window. *Proc. Natl. Acad. Sci. USA* **2011**, *108*, 8943–8949. [CrossRef] [PubMed]

13. Prakash, S.; Malhotra, M.; Shao, W.; Tomaro-Duchesneau, C.; Abbasi, S. Polymeric nanohybrids and functionalized carbon nanotubes as drug delivery carriers for cancer therapy. *Adv. Drug Deliv. Rev.* **2011**, *63*, 1340–1351. [CrossRef] [PubMed]

14. Arsawang, U.; Saengsawang, O.; Rungrotmongkol, T.; Sornmee, P.; Wittayanarakul, K.; Remsungnen, T.; Hannongbua, S. How do carbon nanotubes serve as carriers for gemcitabine transport in a drug delivery system? *J. Mol. Graph. Model.* **2011**, *29*, 591–596. [CrossRef] [PubMed]

15. Foldvari, M.; Bagonluri, M. Carbon nanotubes as functional excipients for nanomedicines: II. Drug delivery and biocompatibility issues. *Nanomed. Nanotechnol. Biol. Med.* **2008**, *4*, 183–200. [CrossRef] [PubMed]

16. Karchemski, F.; Zucker, D.; Barenholz, Y.; Regev, O. Carbon nanotubes-liposomes conjugate as a platform for drug delivery into cells. *J. Control. Release* **2012**, *160*, 339–345. [CrossRef] [PubMed]

17. Wu, H.; Liu, G.; Wang, X.; Zhang, J.; Chen, Y.; Shi, J.; Yang, H.; Hu, H.; Yang, S. Solvothermal synthesis of cobalt ferrite nanoparticles loaded on multiwalled carbon nanotubes for magnetic resonance imaging and drug delivery. *Acta Biomater.* **2011**, *7*, 3496–3504. [CrossRef] [PubMed]

18. Ji, Z.; Lin, G.; Lu, Q.; Meng, L.; Shen, X.; Dong, L.; Fu, C.; Zhang, X. Targeted therapy of SMMC-7721 liver cancer *in vitro* and *in vivo* with carbon nanotubes based drug delivery system. *J. Colloid Interface Sci.* **2012**, *365*, 143–149. [CrossRef] [PubMed]

19. Ye, Y.; Ju, H. Rapid detection of ssDNA and RNA using multi-walled carbon nanotubes modified screen-printed carbon electrode. *Biosens. Bioelectron.* **2005**, *21*, 735–741. [CrossRef] [PubMed]

20. Shakhmaeva, I.I.; Bulatov, E.R.; Bondar, O.V.; Saifullina, D.V.; Culha, M.; Rizvanov, A.A.; Abdullin, T.I. Binding and purification of plasmid DNA using multi-layered carbon nanotubes. *J. Biotech.* **2011**, *152*, 102–107. [CrossRef] [PubMed]

21. Awasthi, K.; Singh, D.P.; Singh, S.K.; Dash, D.; Srivastava, O.N. Attachment of biomolecules (protein and DNA) to amino-functionalized carbon nanotubes. *New Carbon Mater.* **2009**, *24*, 301–306. [CrossRef]

22. Krajcik, R.; Jung, A.; Hirsch, A.; Neuhuber, W.; Zolk, O. Functionalization of carbon nanotubes enables non-covalent binding and intracellular delivery of small interfering RNA for efficient knock-down of genes. *Biochem. Biophys. Res. Commun.* **2008**, *369*, 595–602. [CrossRef] [PubMed]

23. Yang, K.; Wu, W.; Jing, Q.; Zhu, L. Aqueous adsorption of aniline, phenol, and their substitutes by multi-walled carbon nanotubes. *Environ. Sci. Technol.* **2008**, *42*, 7931–7936. [CrossRef] [PubMed]

24. Rao, G.P.; Lu, C.; Su, F. Sorption of divalent metal ions from aqueous solution by carbon nanotubes: A review. *Sep. Purif. Technol.* **2007**, *58*, 224–231. [CrossRef]

25. Mauter, M.S.; Elimelech, M. Environmental applications of carbon-based nanomaterials. *Environ. Sci. Technol.* **2008**, *42*, 5843–5859. [CrossRef] [PubMed]

26. Global Carbon Nanotubes Market—Industry Beckons. Available online: http://www.nanowerk.com/spotlight/spotid=23118.php (accessed on 28 January 2016).

27. Fares, M.M.; Al-Shboul, A.M. Stimuli pH-responsive (*N*-vinylimidazole-coacryloylmorpholine) hydrogels; meso- and nano-porous scaffolds. *J. Biomed. Mater. Res. Part A* **2012**, *100*, 863–871. [CrossRef] [PubMed]

28. Fares, M.M.; Othman, A.A. Smart pH-sensitive alternating copolymers of (methylacrylamide-hydroxyethylmethacrylate); kinetic and physical properties. *J. Macromol. Sci. Part A* **2009**, *47*, 61–70. [CrossRef]

29. Fares, M.M.; El-Faqeeh, A.S. Thermal and thermoxidative degradations of starch and thermosensitive starch-g-BAM copolymers. *J. Therm. Anal. Calorim.* **2005**, *82*, 161–166. [CrossRef]

30. Fares, M.M.; Othman, A.A. Lower critical solution temperature determination of smart, thermosensitive *N*-isopropylacrylamide-alt-2-hydroxyethyl methacrylate copolymers: Kinetics and physical properties. *J. Appl. Polym. Sci.* **2008**, *110*, 2815–2825. [CrossRef]

31. Fares, M.M. Graft copolymerization onto Chitosan-II. Grafting of acrylic acid and hydrogel formation. *J. Polym. Mater.* **2003**, *20*, 75–82.

32. Fares, M.M.; Abul-Haija, Y.; Assaf, S. Pectin grafted poly(vinylpyrrolidone); optimization and *in vitro* controllable theophylline drug release. *J. Appl. Polym. Sci.* **2010**, *117*, 1945–1954. [CrossRef]

33. Fares, M.M.; Sheikh Salem, M.; Khanfar, M. Inulin and poly(acrylic acid) grafted inulin for dissolution enhancement and preliminary controlled release of poorly water-soluble irbesartan drug. *Int. J. Pharm.* **2011**, *410*, 206–211. [CrossRef] [PubMed]

34. Fares, M.M.; Salem, M.S. Dissolution enhancement of curcumin via curcumin-prebiotic inulin nanoparticles. *Drug Dev. Ind. Pharm.* **2015**, *41*, 1785–1792. [CrossRef] [PubMed]

35. Khanfar, M.; Fares, M.M.; Salem, M.S.; Qandil, A. Mesoporous silica based macromolecule for dissolution enhancement of Irbesartan drug using pre-adjusted pH method. *Microporous Mesoporous Mater.* **2013**, *123*, 22–28. [CrossRef]

36. Fares, M.M.; Abu Al-Rub, F.A.; Kandah, M.; Allaboun, H. Environmentally-friendly copolymeric beads of chlorella vulgaris and poly(methacrylamide) gfted aligic acid di-block copolymers for biosorption of zinc ions. *Polym. Int.* **2013**, *62*, 1179–1186.

37. Fares, M.M.; Tahboub, Y.R.; Khatatbeh, S.T.; Abul-Haija, Y.M. Eco-friendly, vascular shape and interpenetrating poly(acrylic acid) grafted pectin hydrogels; biosorption and desorption investigations. *J. Polym. Environ* **2011**, *19*, 431–439. [CrossRef]

38. Fares, M.M.; Maayta, A.K.; Al-Mustafa, J.A. Synergistic corrosion inhibition of aluminum by poly(ethylene glycol) and ciprofloxacin in acidic Media. *Adhes. Sci. Technol.* **2013**, *27*, 2495–2506. [CrossRef]

39. Fares, M.M.; Maayta, A.K.; Al-Qudah, M.M. Polysorbate-20 adsorption layers below and above critical micelle concentration; cloud point and inhibitory role investigations at the solid/liquid interfaces. *Surf. Interface Anal.* **2013**, *45*, 906–912. [CrossRef]

40. Fares, M.M.; Maayta, A.K.; Al-Mustafa, J.A. Corrosion inhibition of iota-carrageenan natural polymer on aluminum in presence of zwitterion mediator in HCl media. *Corros. Sci.* **2012**, *65*, 223–230. [CrossRef]

41. Fares, M.M.; Maayta, A.K.; Al-Qudah, M.M. Pectin as promising green inhibitor of aluminum in hydrochloric acid solution. *Corros. Sci.* **2012**, *60*, 112–117. [CrossRef]

42. Wiltsey, C.; Christiani, T.; Williams, J.; Scaramazza, J.; van Sciver, C.; Toomer, K.; Sheehan, J.; Branda, A.; Nitzl, A.; England, E.; *et al.* Thermogelling bioadhesive scaffolds for intervertebral disk tissue engineering: Preliminary *in vitro* comparison of aldehyde-based *versus* alginate microparticle-mediated adhesion. *Acta Biomater.* **2015**, *16*, 71–80. [CrossRef] [PubMed]

43. Zouboulis, A.; Katsoyiannis, I.A. Arsenic removal using iron oxide loaded alginate beads. *Ind. Eng. Chem. Res.* **2002**, *41*, 6149–6155. [CrossRef]

44. Katsoyiannis, I.A.; Zouboulis, A. Removal of uranium from contaminated drinking water: A mini review of available treatment methods. *Desalination Water Treat.* **2013**, *51*, 2915–2925. [CrossRef]

45. Rasheed, A.; Howe, J.Y.; Dadmun, M.D.; Britt, P.F. The efficiency of the oxidation of carbon nanofibers with various oxidizing agents. *Carbon* **2007**, *45*, 1072–1080. [CrossRef]

46. Papajová, E.; Bujdos, M.; Chorvát, D.; Stach, M.; Lacík, I. Method for preparation of planar alginate hydrogels by external gelling using an aerosol of gelling solution. *Carbohydr. Polym.* **2012**, *90*, 472–482. [CrossRef] [PubMed]

47. Chen, C.; Liang, B.; Ogino, A.; Wang, X.; Nagatsu, M. Oxygen functionalization of multiwall carbon nanotubes by microwave-excited surface-wave plasma treatment. *J. Phys. Chem. C* **2009**, *113*, 7659–7665. [CrossRef]

48. Scheibe, B.; Borowiak-Palen, E.; Kalenczuk, R.J. Oxidation and reduction of multiwalled carbon nanotubes—Preparation and characterization. *Mater. Charact.* **2010**, *61*, 185–191. [CrossRef]

49. Zhao, C.; Ji, L.; Liu, H.; Hu, G.; Zhang, S.; Yang, M.; Yang, Z. Functionalized carbon nanotubes containing isocyanate groups. *J. Solid State Chem.* **2004**, *177*, 4394–4398. [CrossRef]

50. Socrates, G. *Infrared and Raman Characteristic Group Frequencies: Tables and Charts*, 3rd ed.; Wiley: New York, NY, USA, 2001.

51. Miralles, P.; Johnson, E.; Church, T.L.; Harris, A.T. Multiwalled carbon nanotubes in alfalfa and wheat: Toxicology and uptake. *J. R. Soc. Interface* **2012**, *9*, 3514–3527. [CrossRef] [PubMed]

52. Tian, L.; Ghosh, D.; Chen, W.; Pradhan, S.; Chang, X.; Chen, S. Nanosized carbon particles from natural gas soot. *Chem. Mater.* **2009**, *21*, 2803–2809. [CrossRef]